Completing Our Universe:
Direct Detection of Dark Matter with Cryogenic Liquid Noble Gases

Michelle J. Price*

Dr. Katsushi Arisaka

Research Experience for Undergraduates,
University of California, Los Angeles

Abstract

Leading postulations in supersymmetry indicate that the Weakly Interacting Massive Particle (WIMP) accounts for the bulk of mass observed as dark matter in the Universe. Cryogenic liquid noble detectors are expected to discover these particles within the next two years. This experiment investigates the limits of detectors designed around the XENON10 prototype in determination of WIMP mass and interacting cross section, incorporating the latest detector capability information. Phase I of this experiment predicts the bounds with which WIMP mass can be determined for both liquid Xenon (LXe) and liquid Argon (LAr) detector targets for a fixed, best-motivated cross section of $10^{-44}\,\mathrm{cm}^2$ and detector scales of .1, 1, 10 and 100 tons. Monte Carlo simulations using the C++ - based Root histogramming package fit 21 000 generated energy spectra and isolate the mass-dependent exponential parameter. It was determined that upper and lower limits could be set for small masses under $100 - 200$ GeV, with larger detectors exhibiting greater determination ranges and LXe generally outperforming LAr. Phase II of the experiment abandons the fixed cross section assumption, using analytical functions to place best-scenario bounds on how well both WIMP mass and interacting cross section could be determined for both LXe and LAr targets with detectors of .1, 1 and 10 ton target masses. Phase II uses Root to compare several analytically generated experimental energy spectra with nearly a million comparison spectra, computing the Chi Square of each base (experimental) histogram with each comparison histogram to yield confidence-level bounds for mass and cross section. Larger detectors were able to confine probable mass and cross section combinations to much narrower bands than 100 kg-scale detectors but still resulted in infinite mass-cross section combinations for WIMPs with mass greater than about 100 GeV. This study underscores the value of cryogenic liquid noble dark matter detectors on the ton scale and larger in order to discover the basic parameters of the particles that dominate our Universe.

* Gustavus Adolphus College, St. Peter, MN

Introduction

Dark Matter Basics

Flat galactic rotation curves [1, 2, 3], large-scale structure in the universe [4, 5] and surprising results from gravitational lensing studies [6] are three of many peculiarities indicating the existence of large amounts of unseen "dark" matter in the Universe.

A plethora of models and theories regarding the composition of this matter have been formulated, ranging from mathematical adjustments of accepted gravitational theory to high densities of non-luminous baryonic dark matter [7], neutrinos [8, 9], hypothetical gravitinos and more (for a more complete list see [8]). Well-motivated theories from supersymmetry predict that this dark matter takes the form of Weakly Interacting Massive Particles (WIMPs) that can be discovered with direct detectors [10, 11, 12, 13, 14, 15, 16].

Theory provides only very general estimations for the mass (in the range of 10 to 1000 GeV or so [17]) and interacting cross section (about 10^{-44} cm^2 [18]) of the WIMP. Phase I of this experiment investigates the precision with which mass can be approximated for a fixed most-probable cross section via energy spectrum analysis. Phase II abandons the fixed cross section assumption to observe how well both mass and cross section can be determined at various detector scales, again relying on energy spectrum analysis.

Parameters for this experiment were chosen to reflect the capabilities of detectors relevant to the UCLA dark matter group; namely, XENON10, LUX and larger-scale designs based on these prototypes.

Cryogenic Liquid Noble Detectors

UCLA's dark matter group is working with a detector design used for three scales of detection representing the past, present and future of direct detection attempts.

XENON10   [19]

XENON10 is an international dark matter detection collaboration that ran an experiment at Gran Sasso National Laboratory, Italy from 6 October 2006 to 14 February 2007. The XENON10 detector has inner dimensions of 20 cm diameter x 15 cm height and holds 15 kg liquid Xenon for a fiducial mass of 5.4 kg after several cm self-shielding. Eighty-nine Hamamatsu R8520 photomultiplier tubes (PMTs) are incorporated in the design. Electrons are drifted with a .73 kV/cm field and the entire ensemble is shielded with 20cm polyethylene and 20 cm lead.

The XENON10 group collected 58.6 days of data after cuts. Effectiveness of the XENON10 design at registering internal activity was verified and the group reported at a 90% CL that WIMP cross section is below 8.8 x 10^{-44} cm^2 for a 100 GeV WIMP.

LUX   [20]

The Large Underground Xenon collaboration will incorporate new technologies such as an active water shield to the XENON10 design to create a larger, more sensitive detector capable of probing predicted WIMP cross sections (see [18]). The LUX detector will have dimensions of 40 cm diameter x 60 cm height and will hold 300 kg LXe for a 100 kg fiducial mass. LUX will be equipped with 120 Hamamatsu

R8778 PMTs and a .2-1 kV/cm electron drift field. It will detect WIMPs with cross sections as low as 7×10^{-46} cm^2.

Larger Detectors

The UCLA group is also investigating how a detector of the XENON10 design could be scaled up to a multi-ton fiducial mass. The experiments that follow include predictions of WIMP information that could be determined from a detector of this size relative to previously- and currently- explored scales.

The WIMP Energy Spectrum [21]

Both phases of the experiment rely on theoretically predicted energy spectra for WIMP interactions in various materials. The differential energy spectrum for nuclear recoils from the weak interaction is of the basic form

$$dR/dE_R = R_o/E_o r \ e^{-E_R/E_o r} \qquad (1)$$

with R = event rate per unit mass, E_R = recoil energy, R_o = total event rate, E_o = most probable incident WIMP kinetic energy and r = kinematic factor $(4M_D M_T)/(M_D + M_T)^2$ for WIMP mass M_D and target nucleus mass M_T. Order-of-magnitude approximations thus indicate recoil energies in the 1-100 keV range for $10 < M_D < 1000$ GeV.

Observed energy spectra are complicated by additional factors; for example, finite nuclear size contributes to the nuclear form factor correction. Momentum transfer of the weak interaction is described by

$$q = (2M_T E_R)^{1/2} \qquad (2)$$

with a corresponding wavelength

$$\lambda = h/q \qquad (3)$$

with h = Planck's constant. Effective cross-section falls with larger q when λ becomes comparable to the nuclear radius, leading to the solid sphere form factor

$$F = 3[\sin(qr_n) - qr_n\cos(qr_n)]/(qr_n)^3 \qquad (4)$$

WIMP spin dependence would complicate the nuclear form factor in addition to further energy spectrum deformation. The Earth-bound detector location is also expected to affect the differential spectrum as it orbits the sun, which is itself moving with respect to the galaxy. Variations in detector efficiency for nuclear and electron (background) recoils, a mixed or "dirty" target with multiple M_T values and instrumental effects will appear in the observed spectrum as well, making the modified energy spectrum

$$dR/dE|_{obs} = R_o S(E)F^2(E)I \qquad (5)$$

where I accounts for WIMP spin, F(E) is the nuclear form factor and S(E) the spectral function modified to include other effects. The following analysis assumes a differential energy spectrum

$$dR/dE|_{obs} = (1) \times (4)^2 \qquad (6)$$

(the base spectrum (1) multiplied by the form factor squared $(4)^2$) for a good spectral approximation (see Fig 1).

It should also be noted that observed WIMP event rates are directly proportional to the interacting cross section of the particle. If, for instance, 13 000 events are expected for 10 ton-yr observation of 100 GeV WIMPs with a cross sections 10^{-44} cm^2, one would expect only 1 300 events if the 100 GeV WIMP had a cross section of 10^{-45} cm^2.

Xe Energy Spectrum @ 100 GeV, 10-44 cm2

LXe Target
100 GeV WIMPs
~13000 Events for 10 ton -yr
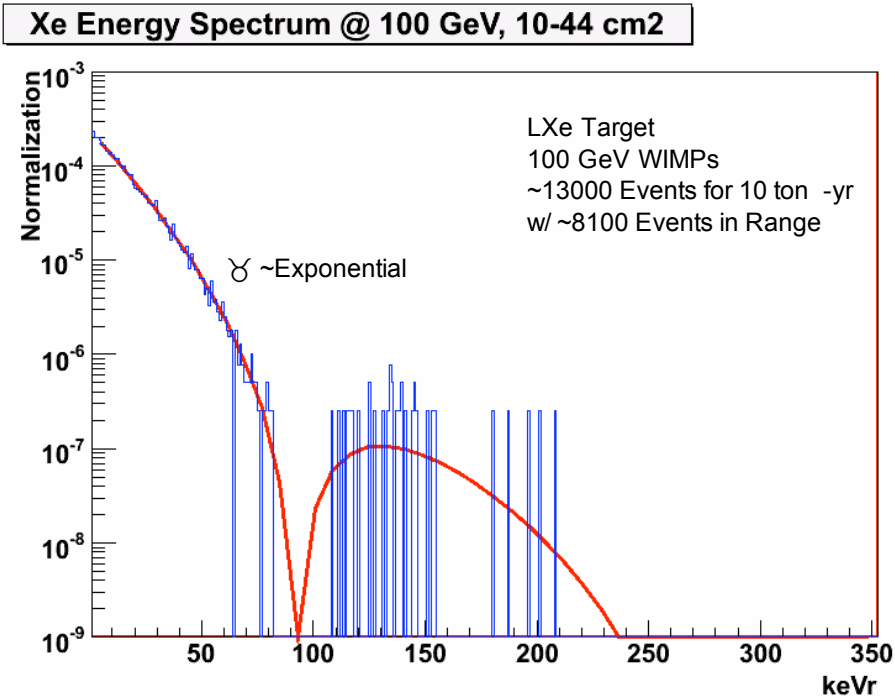w/ ~8100 Events in Range

♉ ~Exponential

Figure 1: An example energy spectrum for a 100 GeV, 10^{-44} cm^2 WIMP and 10 ton-yr detection with a LXe target. The red line is the theoretically expected spectrum (6) and the superimposed blue histogram is a Monte Carlo simulation of experimentally detected events.

Experimental Spectrum Analysis [22, 23]

Experimentally generated WIMP spectra will include a background rate (false WIMP detections) that must be accounted for in spectrum analysis. This is generally accomplished by selecting only the high-event-rate, low-recoil-energy range for analysis such that background signals are negligible compared to the WIMP rate. This experimentally available spectrum segment is indicated in Fig 1 and behaves according to a basic exponential equation

$$dR/dE_R = Ae^{-Ea} \qquad (7)$$

where the parameter a follows the proportionality

$$1/a \; \alpha \; v_o^2/(1 + M_T/M_D)^2 \qquad (8)$$

with v_o = galactic velocity. Fig 2 shows the expected mass dependence of a for a 132 GeV target mass (Xenon), clearly exhibiting greater parameter variation with smaller versus larger masses. Jackson and Gaitskell provide an excellent visualization of basic mass determination behavior in Fig 3 as part of a primarily Si and Ge-based study [22]. Phase I of the experiment reported below attempts to set more meaningful bounds for UCLA's specific cryogenic liquid noble detection techniques by simulating at the best-motivated WIMP cross section (10^{-44} cm^2) and by generating data specific to our detector capabilities.
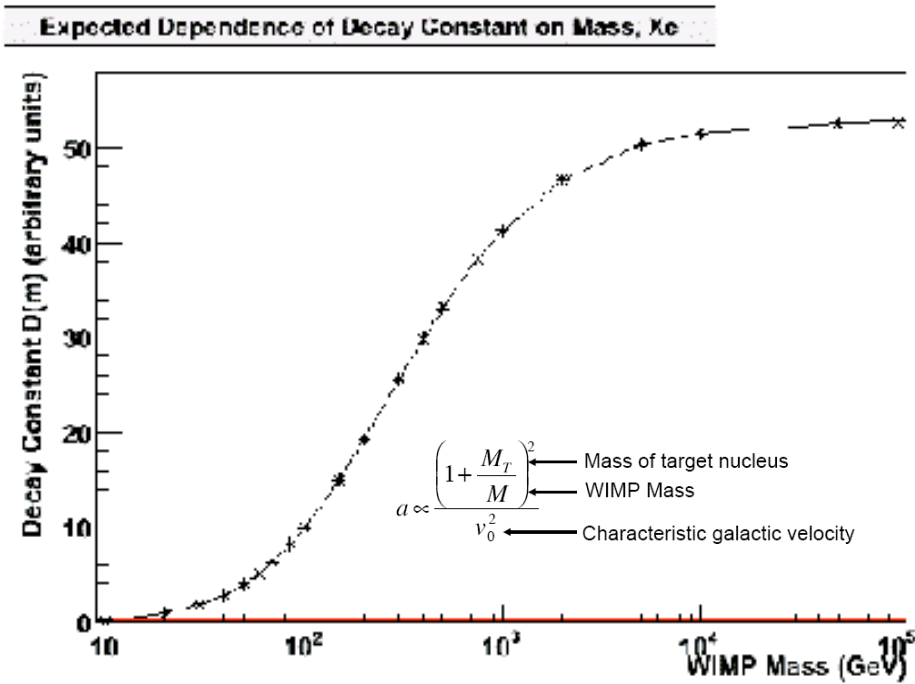
Figure 2: Expected dependence of the exponential decay constant a (see (7)) on WIMP mass for a Xenon target (8). The decay constant is useful in mass determination for ranges where it shows considerable variation (small masses) but becomes constant as WIMP mass dominates target mass.
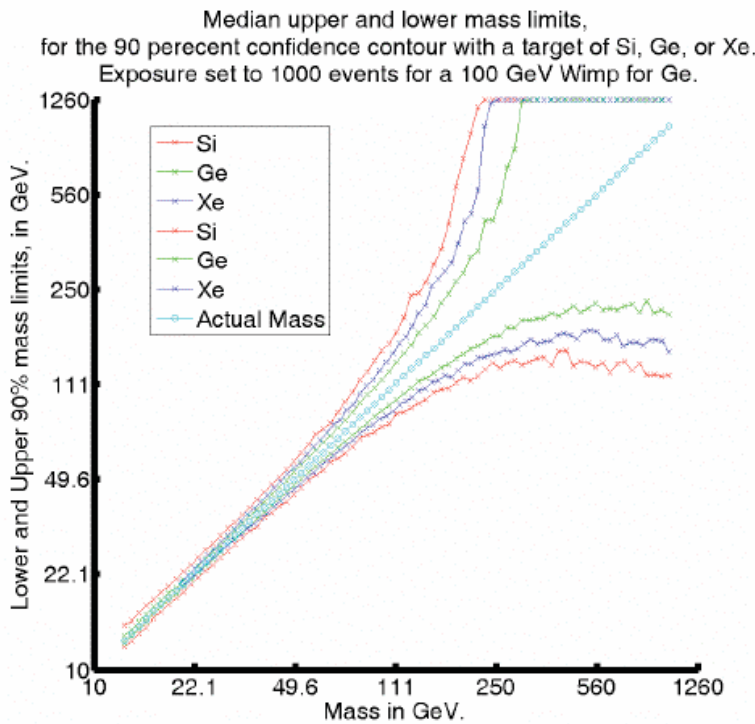

Figure 3: Results from Jackson and Gaitskell's study of mass determination using 1000 events in Ge [22]. Upper bounds can be set in the range from $10 - 100$ or 200 GeV but diverge for large masses. Lower bounds plateau in the same $100 - 200$ GeV range.

WIMP mass determination is complicated by an equally important determination of the particle's interacting cross-section. Expected event rates (proportional to A in (7)) are negatively correlated with mass and are directly proportional to WIMP cross section. For small masses, an unambiguous exponential fit of a coupled with event rate information allows fairly tight bounds to be set on both WIMP mass and cross-section. As M_D increases, however, a becomes constant and no upper mass boundaries can be set. For a known cross section mass could be determined by simple event rate observations, but without this assumption an infinite number of mass-cross section combinations satisfy the spectrum. Figure 4 from the Jackson-Gaitskell study [22] shows this behavior (confirmed in a study by Anne Green [24]) for a 50 000 kg-dy Germanium target exposure. Phase II of this experiment duplicates these studies using energy spectra expected from cryogenic liquid noble gas detectors of the XENON10 prototype.
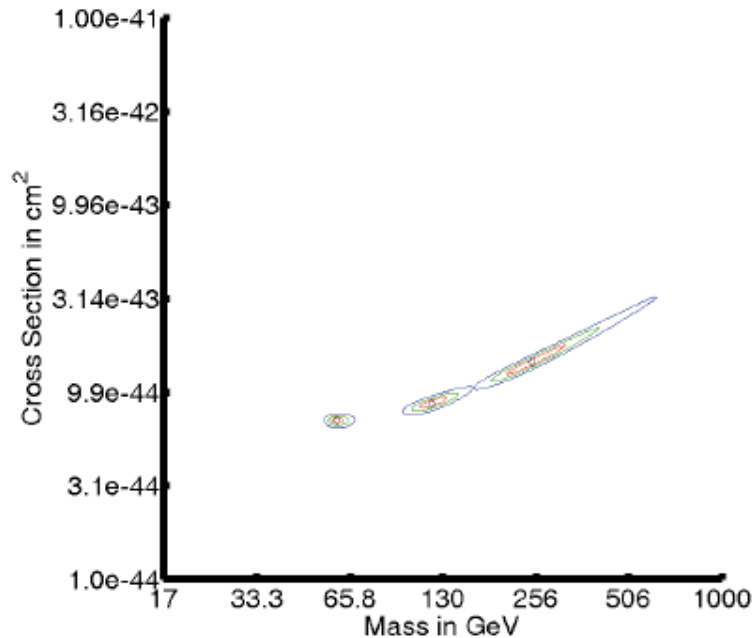

Figure 4: Determination of WIMP mass and cross section with Ge target in a study by Jackson & Gaitskell [22]. Mass determination is found to be quite good for low masses (as depicted by the small probable ranges of the 60 GeV WIMP) but becomes increasingly difficult for masses greater than 100 GeV (120 GeV and 250 GeV, above). Central cross-sections based on observations of 1000 events.

The outcome of these simulations with liquid Xenon (LXe) and liquid Argon (LAr) was expected to closely resemble the findings of [22, 24]. Cryogenic liquid noble detectors are arguably the most feasible option for large-scale detectors of the future. It is critical that the extent to which they can describe WIMPs is verified before resources are allocated to their construction.

Methods & Materials

Phase I: Mass Determination for a Fixed Cross Section

Phase I of the experiment was to determine how well WIMP mass could be constrained through energy spectrum analysis for an assumed cross section of 10^{-44} cm^2 [18] and detector sizes of 0.1, 1, 10 and 100 tons. The analysis was performed via computer Monte Carlo simulation using the C++ programming language and Root histogramming package.

The program was built around a piece of code written by Weichung Ooi and motivated by [21] that generated an energy spectrum according to (6) for a particular target material, WIMP mass and interacting cross section. The energy spectrum was fitted to an exponential function via TF1::Fit("expo", "Q", "R", 4.5, 50) for recoil energies from 4.5 to 50 keVr, as motivated by expected detector capabilities. The exponential parameter (a in (7)) was extracted via TF1::GetParameter(1). Because statistical fluctuation is present in experimental data (and hence Monte Carlo simulation), 1000 energy spectra were generated and fitted to yield a mean, RMS and 90% CL range for the a (specifically $1/a$) parameter. Simulations for the 10 ton detector were executed by running the described program 21 times for each of the masses listed in Table 1. In order to streamline data acquisition, the program was looped over the 21 masses to collect all data in a single run for subsequent detector simulations. The expected number of WIMP events per mass (also found in Table 1) were calculated via another program provided by Weichung Ooi.

Mass (GeV)	No. Events, Xe	No. Events, Ar
10	13508	3039
20	19271	3881
30	21077	4049
40	20808	3966
50	19661	3790
60	18246	3584
70	16832	3380
85	14920	3091
100	14349	2834
150	13308	2193
200	7499	1777
300	5169	1281
400	3936	1000
500	3176	819
600	2661	694
700	2290	601
800	2010	531
900	1790	475
1000	1614	430

Table 1: WIMP mass and expected number of events for Xenon and Argon targets with an assumed cross section of 10^{-44} cm^2 and 10 ton-yr of exposure. Note that Argon interacts at about 25% the rate of Xenon and event rate generally decreases for increasing WIMP mass.

The mean $1/a$ was plotted separately with its 90% and RMS CL values, resulting in graphs like those pictured in Figs 5 and 6. RMS and 90% CL mass determination capability was estimated by observing the mass ranges that fit within the corresponding CL bounds. Horizontal guides were superimposed on the graphs via Microsoft PowerPoint when necessary to aid in mass bound estimation. The expected, maximum and minimum mass determination ranges were recorded manually and plotted using Root (see Figs 7 – 10).

Because the WIMP event rate is directly proportional to the interacting cross section, simulation for a 1 ton detector recording WIMP events at an assumed cross section of 10^{-44} cm^2 is identical to that for a 10 ton detector and 10^{-45} cm^2 WIMPs. The experimenter found it more expedient to assume a 10 ton-yr detector for all simulations, mimicking varying detector sizes by changing the cross section and event rate parameters. The 100 ton-yr exposure simulation, for example, assumed a 10 ton-yr exposure, 10^{-43} cm^2 cross section and ten times the WIMP event listed in Table 1.

Phase II: Mass and Cross Section Determination

Best-scenario, simultaneous determination of WIMP mass and cross section was accomplished by comparing the goodness of fit of several analytically generated base spectra with a nearly a million comparison spectra.

The Phase II program made extensive use of the histogramming capabilities of Root. The analytical energy spectrum function (6) was used to create five base histograms for 20, 50, 100, 200 and 500 GeV WIMPs, representing potential detector data. The histograms had 23 bins, with data generated in the $4 - 50$ and $20 - 100$ keVr range for LXe and LAr, respectively and distributed with no statistical fluctuation in the bins.

The program scanned masses linearly from $10 - 1000$ GeV in 1 GeV increments and 1000 cross sections linearly from an order of magnitude above the base cross section to an order of magnitude below. For each of these 990 000 mass and cross section combinations, a corresponding comparison energy spectrum was generated, also analytically according to (6). A chi square was calculated between the comparison spectrum and each base spectra separately by summing (baseBinContent – comparisonBinContent)^2 / baseBinContent over all the bins. The lowest chi square of the five was converted to a confidence level via TMath::Prob(ChiSquare, 2) with the number 2 representing the number of parameters being investigated (mass and cross section). The value 1 – confidence level was separated into 10 linearly spaced color bins corresponding to 10% CL increments and plotted via the Root TH2F histogram function.

The experimenter once again found it more convenient to mimic the exposures of various detector sizes by adjustment of cross section and event rate information.

These programs were designed to be run on any Root-compatible terminal. The figures below were created by runs on the computer Ike and members of the Auger cluster (all located in Knudsen 4-162, UCLA) from July-August 2007.
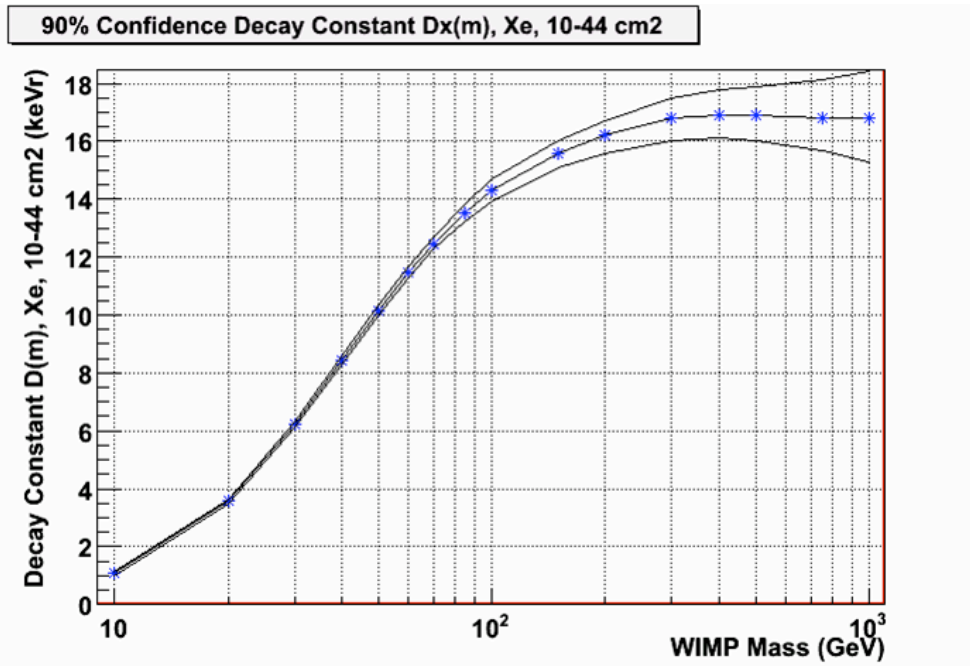
Figure 5: Inverse decay constant for energy spectra generated from 10 ton-yr data collection with a Xenon target mass. The central line with blue asterisks is the mean $1/a$, while the points directly above and below the stars (connected with smooth lines) represent the 90% CL range for $1/a$.
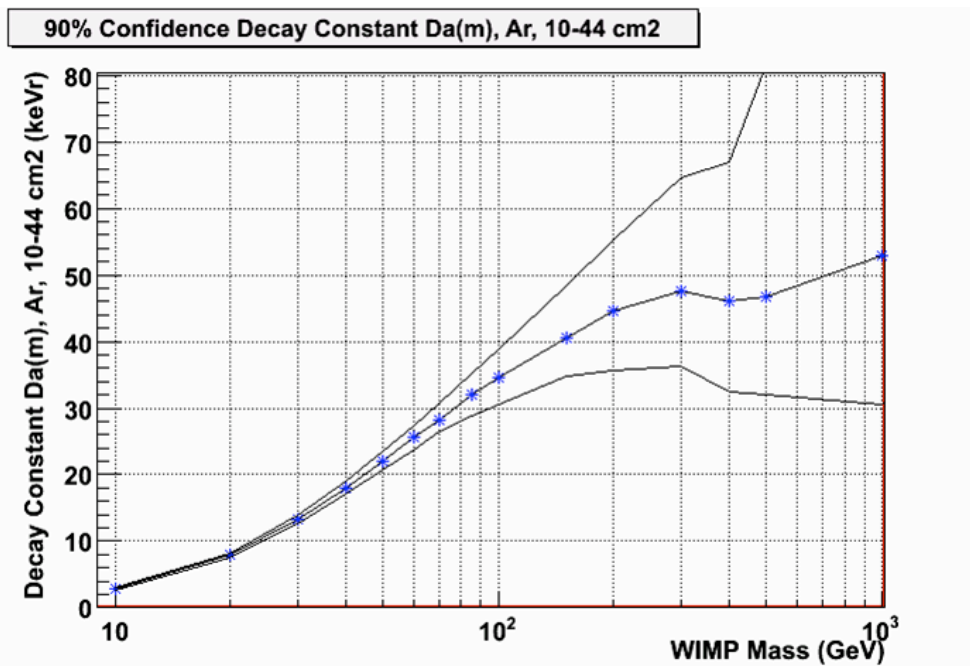

Figure 6: Inverse decay constant for energy spectra generated from 10 ton-yr data collection with an Argon target mass. The mean $1/a$ is the central line with blue asterisks, with the 90% CL range given by the points directly above and below the stars (connected with smooth lines). Note that the 90% CL bounds for an Ar target deviate further from the mean for the same target exposure.

11

Results

Phase I: Mass Determination for a Fixed Cross Section

Phase I of the experiment yielded the four mass vs mass graphs found in Figs 7 – 10. These figures show the range with which WIMP mass can be determined (y axis) for given test masses (x axis) assuming various cross sections/exposures. The figures show fairly precise mass approximation capabilities at the lower end of the mass scale where the RMS and 90% CL bounds are very close to the actual mass line (black stars). As WIMP mass increases, determination capability deteriorates as is demonstrated by the divergence of upper CL bounds and the plateau of lower CL bounds.
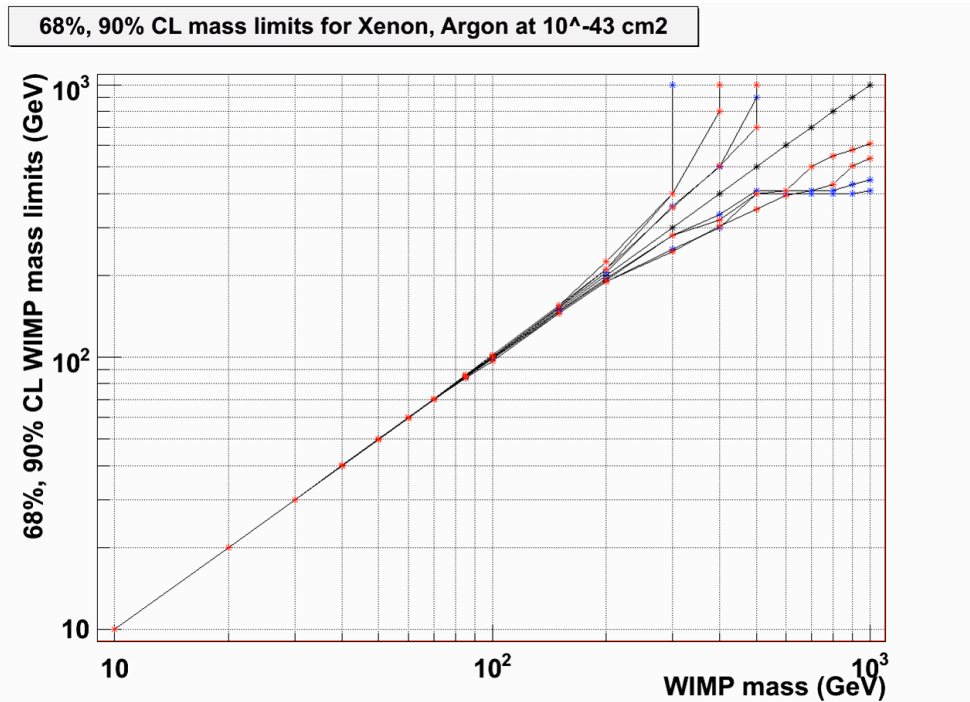

Figure 7: Mass determination capability for 100 ton-yr target exposure and 10^{-44} cm^2 WIMP cross section or 10 ton-yr exposure and 10^{-43} cm^2 cross section. The black stars represent actual WIMP masses with blue and red stars giving the approximation capabilities for LXe and LAr, respectively. Both 90% and RMS CL data are shown, with 90% CL points straying further from the actual mass.
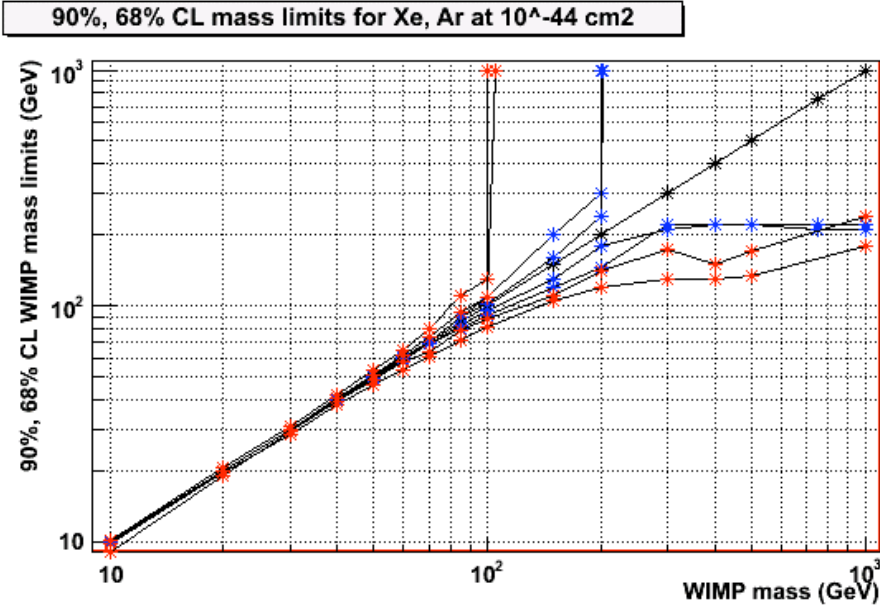
Figure 8: Mass determination capability for 10 ton-yr target exposure and 10^{-44} cm^2 WIMP cross section. The straight line represents real WIMP masses with blue and red stars giving the approximation capabilities for LXe and LAr, respectively. 68%, 90% CL data are shown.
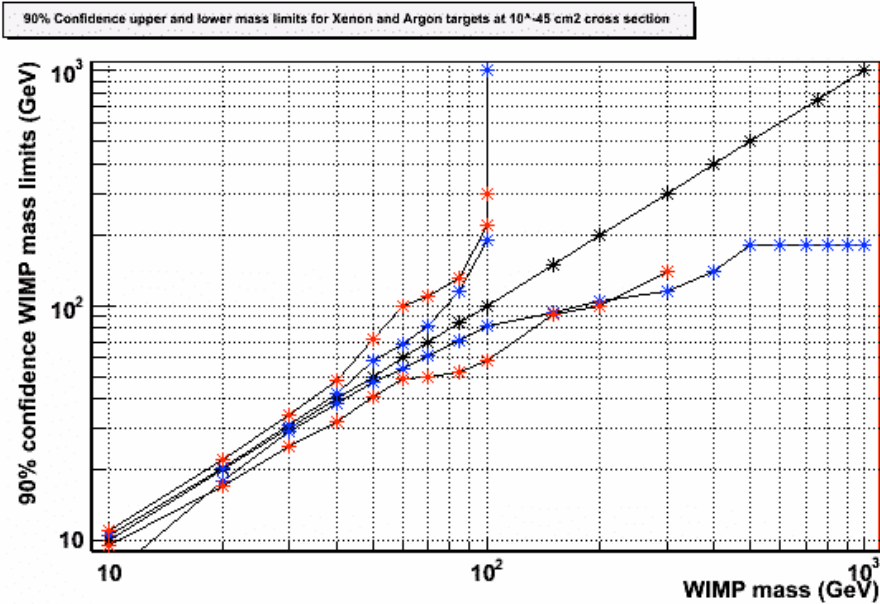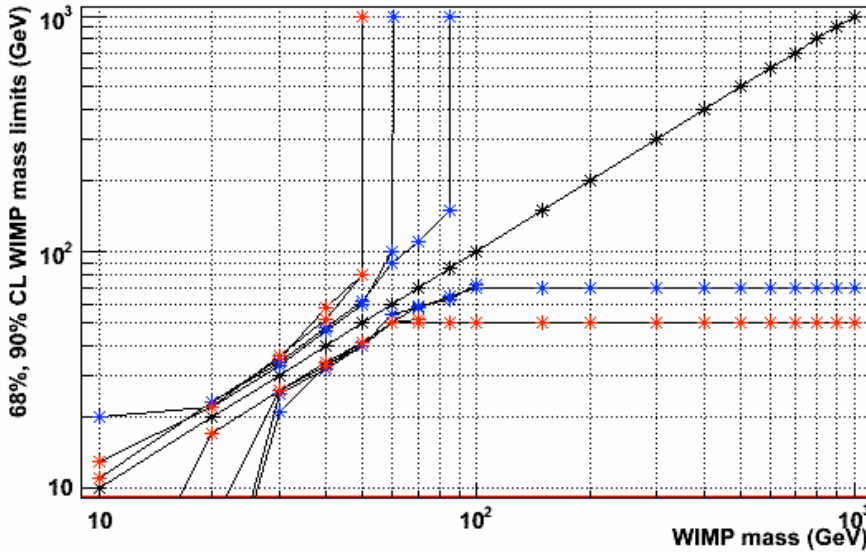

Figure 9: Mass determination capability for 1 ton-yr target exposure and 10^{-44} cm^2 or 10 ton-yr exposure and 10^{-45} cm^2 WIMP cross section. The straight line represents real WIMP masses with blue and red stars giving the approximation capabilities for LXe and LAr, respectively. 90% CL data are shown.

Figure 10: Mass determination capability for 100 kg-yr target exposure and 10^{-44} cm^2 or 10 ton-yr exposure and 10^{-46} cm^2 WIMP cross section. The straight line with black stars represents real WIMP masses with blue and red stars giving the approximation capabilities for LXe and LAr, respectively. Both 90% and RMS CL data are shown, with 90% CL points straying further from the actual mass.

Phase II: Mass and Cross Section Determination

Determination of both mass and cross section via analytical energy spectrum generation and analysis resulted in the parameter determination bounds for LXe targets shown in Figures 11 – 13. The color scales for these graphs are 1 – CL, meaning that for the energy spectra generated in the program there is a 90% chance that actual WIMP masses and cross sections for each base spectra lie within the multicolored circles, ellipses and slashes pictured. As with Phase I data, determination capabilities are fairly good for small target masses (indicated by the small multicolored areas for WIMPs of small masses) but expand to infinite mass-cross section combinations for larger masses. Increased exposures provide for narrower boundaries but do not eliminate the mass-cross section equivalence for high-mass energy spectra.

Simulations of detectors using LAr targets were performed as well, with resulting mass-cross section resolutions given in Figures 14 – 16.
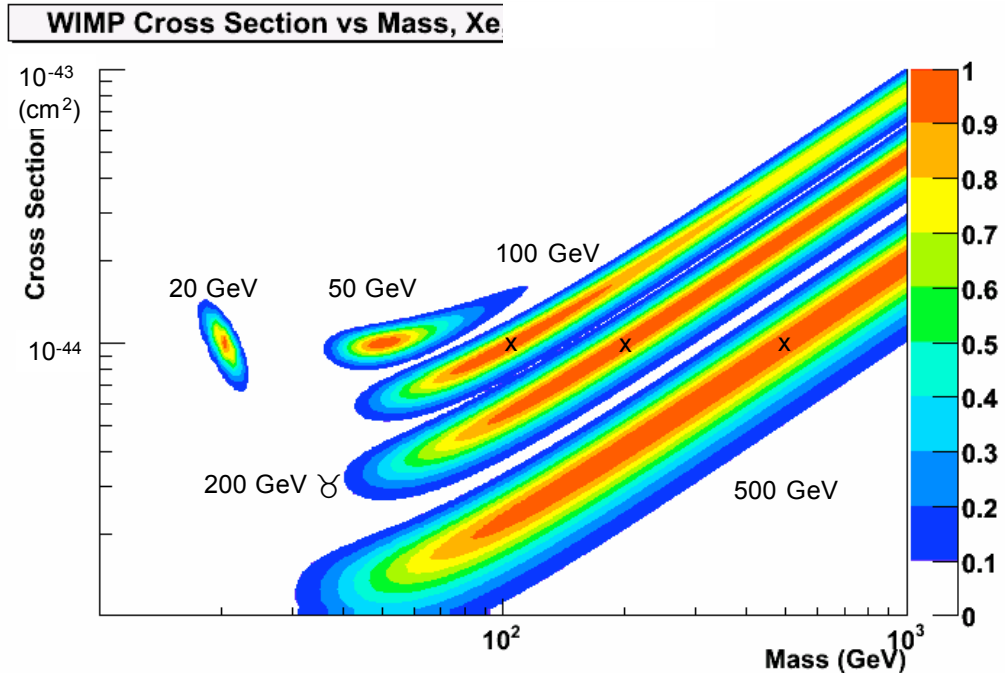
13

Fig 11: Analytical (best-scenario) mass and cross section determination capability for 100 kg-yr Xe target exposure and a 10^{-44} cm^2 WIMP cross section or 10 ton-yr exposure and a 10^{-46} cm^2 WIMP cross section. The color scale is of $1 - CL$ so that there is a 90% probability that (for instance) a 20 GeV WIMP will have parameters within the multicolored ellipse labeled "20 GeV."
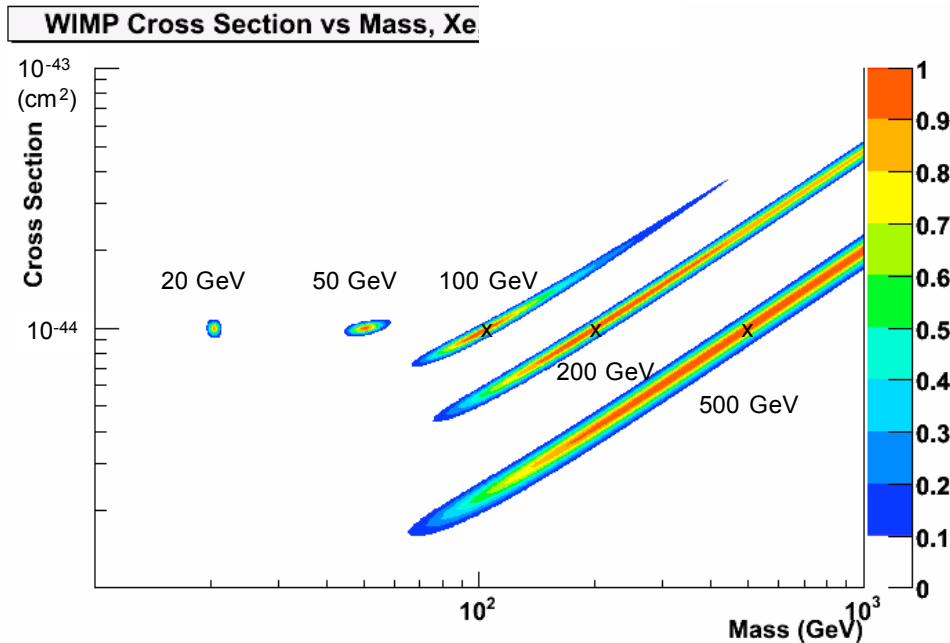

Fig 12: Best-scenario mass and cross section determination capability for 1 ton-yr Xe target exposure and ~10^{-44} cm^2 WIMP cross section or 10 ton-yr exposure and a 10^{-45} cm^2 WIMP cross section. The $1 - CL$ color scale indicates a 90% probability that a WIMP will have parameters within its respective bounds.
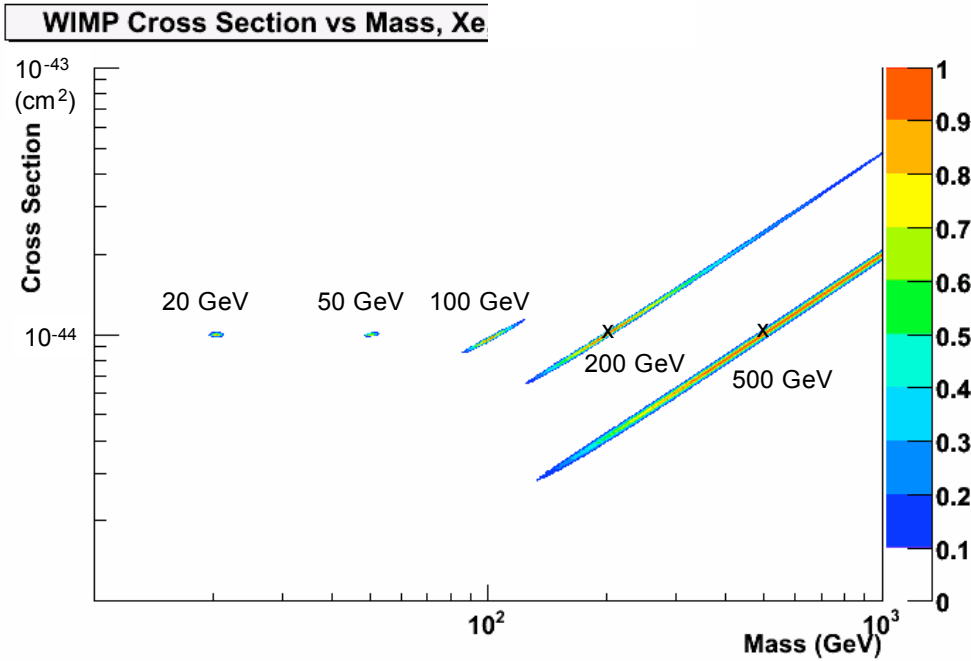
14

Fig 13: Best-scenario mass and cross section determination capability for 10 ton-yr Xe target exposure and ~10^{-44} cm^2 WIMP cross section. The 1 – CL color scale indicates a 90% probability that (for instance) a 20 GeV WIMP will have parameters within the multicolored ellipse labeled "20 GeV."

Figure 14: Best-scenario mass and cross section determination capability for 10 ton-yr Ar target exposure and ~10^{-44} cm^2 WIMP cross section. The 1 – CL color scale indicates a 90% probability that (for instance) a 20 GeV WIMP will have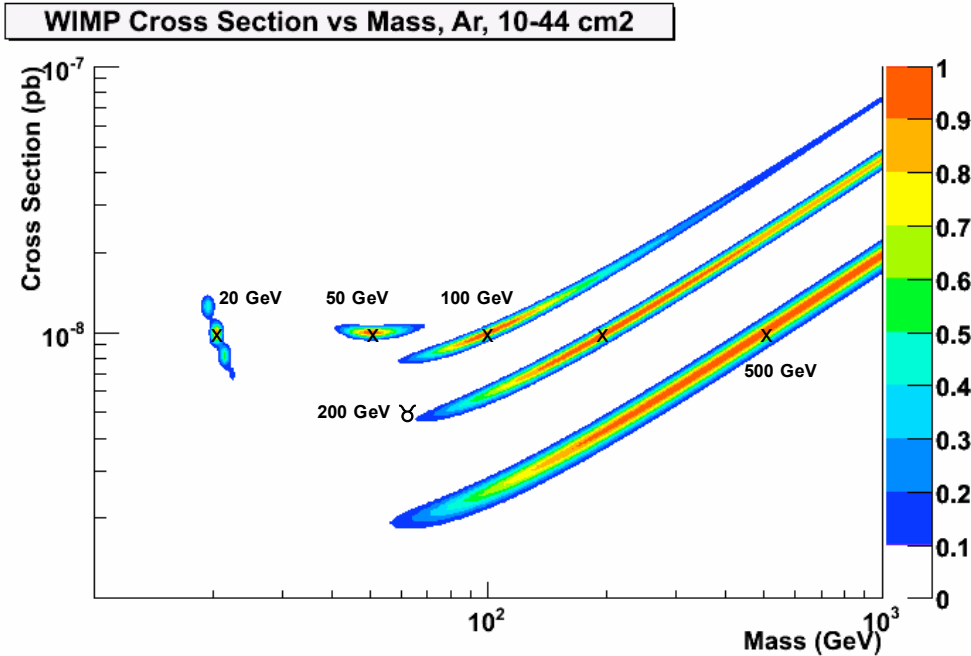 parameters within the multicolored ellipse labeled "20 GeV." The multi-dot pattern for the 20 GeV WIMP is a result of finite parameter intervals.
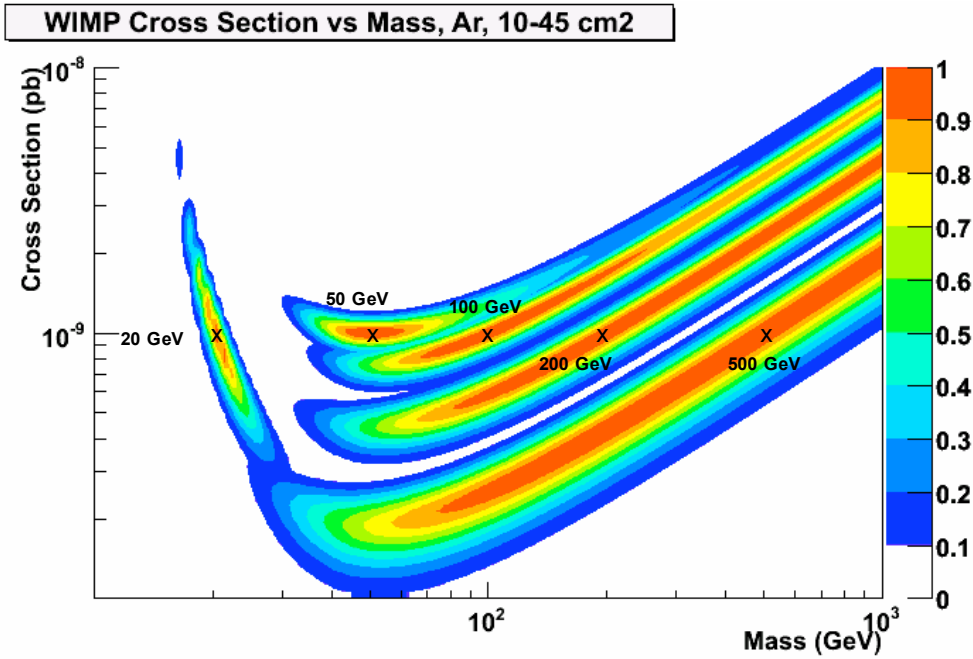
15

Figure 15: Best-scenario mass and cross section determination capability for 1 ton-yr Ar target exposure and ~10^{-44} cm^2 WIMP cross section or 10 ton-yr exposure at 10^{-45} cm^2. The 1 − CL color scale indicates a 90% probability that (for instance) a 20 GeV WIMP will have parameters within the multicolored ellipse labeled "20 GeV." The extra dot near the 20 GeV boundaries is the result of finite scanning intervals.
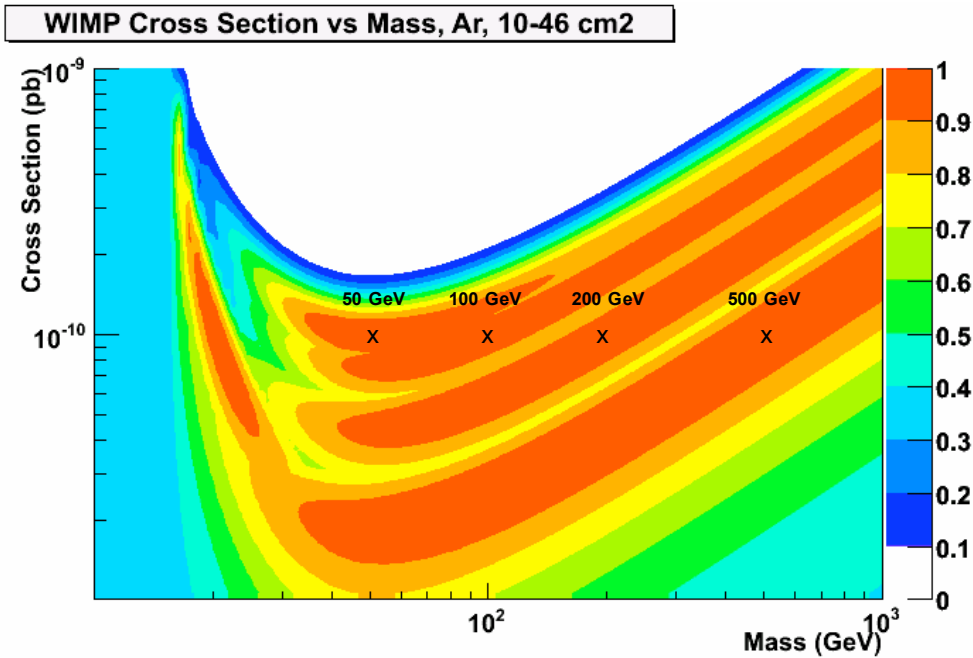

Figure 16: Best-scenario mass and cross section determination capability for 100 kg-yr Ar target exposure and ~10^{-44} cm^2 WIMP cross section or 10 ton-yr exposure and 10^{-46}

cm^2 cross section. The $1 - CL$ color scale indicates a 90% probability that (for instance) a 20 GeV WIMP will have parameters within the multicolored ellipse labeled "20 GeV."

Discussion

Both Phase I and Phase II of the experiment demonstrated fairly precise parameter determination for WIMPs in the mass range $20 - 100$ GeV, depending on the target material and exposure (kg-dy). This is demonstrated in the 100+ GeV divergences for mass determination in Phase I (see Figs 7 – 10) and the small, completely bounded mass-cross section regions in Phase II (see Figs 11 – 14). Superior low-mass resolution was to be expected for at least two reasons. First, the mass-dependant parameter a from (7) is a much better indicator of WIMP mass for low versus high-mass particles (see Fig 2). Besides the more characteristic a parameter, more WIMP events are generally expected for lower masses (see Table 1), leading to less statistical uncertainty for lighter WIMPs.

Phase I in particular demonstrates the value of larger exposures in WIMP mass determination. For an assumed cross section of 10^{-44} cm^2, a detector on the order of 100 kg will only be able to estimate mass at a 90% CL for particles less than 60 GeV (Fig 10). A 10 ton detector, on the other hand, should be able to put 90% CL bounds on WIMPs as massive as 200 GeV (Fig 8).

While Phase I of this study is an interesting application of energy spectrum analysis, it has limited realistic value due to the well-motivated but not yet proven assumption of a 10^{-44} cm^2 WIMP cross section.

More definitive conclusions can be drawn from Phase II, which scans a range of masses and cross sections to match experimental data with the best-fitting comparison energy spectra. This technique utilizes the entire available energy spectrum instead of just the exponential parameter. The much smaller 90% CL bounds for small WIMPs with large exposures supports observations made in Phase I.

Both Phase I and Phase II clearly show the benefits of larger detectors for gathering WIMP information. Detectors on the ton-scale or larger are needed for conclusive WIMP mass and cross section results. Even for very large detectors, however, energy spectra will eventually show redundancy with infinite mass-cross section combinations manifested in the divergence of Phase I data (Figs 7 – 10) and lines of infinite combinations in Phase II data (Figs 11 – 16).

Determination capabilities for LXe and LAr targets differ substantially, perhaps primarily due to the higher detection rate for LXe versus LAr targets (see Table 1, about a factor of four). The effects of the less detailed energy spectra this generates can be traced through the experiment; for instance, Figs 5 and 6 show the precision with which the exponential parameter $1/a$ can be determined. The LAr parameter 90% CL boundaries stray further from the mean than those for LXe, resulting in a lower upper limit for mass determination (see the divergences in Figs 8 – 10). While LAr is less expensive and has proven to be a dependable material in past experimental applications, LXe looks to be the more promising target material of the two for dark matter detection.

The superiority of LXe as a target material appears not to hold for

extremely large detector scales of 100+ tons. This is observed in Fig 7, where LAr is able to provide 90% CL WIMP mass bounds for masses up to 400 GeV as opposed to only 300 GeV for LXe. This likely results from the Ar $1/a$ parameter plateauing at larger decay constants and only appears when statistical fluctuations are small enough. While this is an interesting result worthy of additional study, it is unlikely that detectors on the 100+ ton scale will materialize in the near future.

Phase I of this experiment is an updated version of Jackson and Gaitskell's study [22], expanded to include LAr as a possible target material. While Phase II has been executed for Si and Ge-based detectors [22, 24], this is (as far as the UCLA dark matter group knows) the first attempt at mass-cross section determination simulations for liquid noble gas detectors. Both phases show promising results for the outlook on WIMP studies with cryogenic liquid noble detectors and indicate the need for constructing such detectors on multi-ton scales.

References

[1] Babcock, Horace W. **The Rotation of the Andromeda Nebula**. Lick Observatory Bulletin No. 498. University of California Publications, Astronomy. 4 January 1940.

[2] Banhatti, Dilip G. **Disk galaxy rotation curves and dark matter distribution**. arXiv:astro-ph/0703430. 31 July 2007.

[3] Rubin, Vera C., W. Kent Ford and Norbert Thonnard. **Extended Rotation Curves of High-Luminosity Spiral Galaxies. IV. Systematic Dynamical Properties, Sa → Sc**. *The Astrophysical Journal*. 225. 7 June 1978.

[4] Press, William H. and Paul Schechter. **Formation of Galaxies and Clusters of Galaxies by Self-Similar Gravitational Condensation**. *The Astrophysical Journal*, 187: 425-438. 1 February 1974.

[5] Raha, Bharat and Michael S. Vogeley. **Resource Letter: BE-1: The Beginning and Evolution of the Universe**. arXiv:astro-ph/0706.1565v1. 11 June 2007.

[6] Tortora, C. **Strong Lensing, Dark Matter and H_0 Estimate**. arXiv:astro-ph/0702501v1. 19 February 2007.

[7] Tisserand et al. **Limits on the Macho Content of the Galactic Halo from the EROS-2 Survey of the**

Magellanic Clouds. arXiv:astro-ph/0607207v2. *Astronomy and Astrophysics* man. No. 6017. 19 April 2007.

[8] Bertone, Gianfranco, Dan Hooper and Joseph Silk. **Particle Dark Matter: Evidence, Candidates and Constraints**. arXiv:hep-ph/0404175v2. 31 March 2007.

[9] Strumia, Alessandro and Francesco Vissani. **Neutrino masses and mixings and…** arXiv:hep-ph/0606054v2. 3 May 2007.

[10] Akerib, Daniel S. **Dark Matter: Looking for WIMPs in the Galactic Halo**. *Dept. of Physics, Case Western Reserve University*. 2006+.

[11] Aprile et al. **Scintillation Response of Liquid Xenon to Low Energy Nuclear Recoils**. arXiv:astro-ph/0503621. 18 May 2006.

[12] Bernstein et al. **Research and Development in Active Neutron Tagging for Dark Matter Experiments and Advanced Water Cherenkov Techniques for the Deep Underground Science and Engineering Laboratory (DUSEL)**. 31 October 2006. Available www: www.physics.ucdavis.edu/svoboda/post/ WCTF/DUSEL_RandD_ v2.doc. Accessed 14 August 2007.

[13] Bisset et al. **R & D for Future ZEPLIN**. arXiv:astro-ph/0705.2117v1. 15 May 2007.

[14] **Report on the Direct Detection and Study of Dark Matter**. *The Dark Matter Scientific Assessment Group (DMSAG)*. 5 July 2007.

[15] Formaggio, Joseph A. and C. J. Martoff. **Backgrounds to Sensitive Experiments Underground**. *Annual Review of Nuclear and Particle Science*. Vol. 54. 2004.

[16] Lee, Benjamin W. and Steven Weinberg. **Cosmological Lower Bound on Heavy-Neutrino Masses**. *Physical Review Letters*. Vol. 39 No. 4. 25 July 1977.

[17] Gaitskell, Richard J. **Direct Detection of Dark Matter**. *Annual Review of Nuclear and Particle Science*. Vol 54. 2004.

[18] Roszkowski, Leszek, Roberto Ruiz de Austri and Roberto Trotta. **Implications for the Constrained MSSM from a new prediction for b to s gamma**. zrXiv:hep-ph/0705.2012v1. 14 May 2007.

[19] Angle et al. **First Results from the XENON10 Dark Matter Experiment at the Gran Sasso National Laboratory**. arXiv:astro-ph/0706.0039v1. 31 May 2007.

[20] Arisaka et al. **Construction of the LUX Dark Matter Experiment at the Sanford Underground Science and Engineering Laboratory**. *The LUX Collaboration*. 1 August 2007.

[21] Lewin, J. D. and P. F. Smith. **Review of Mathematics, numerical factors, and corrections for Dark Matter experiments based on elastic nuclear recoil**. *Rutherford Appleton Laboratory*. 29 May 1996.

[22] Jackson, David and Richard Gaitskell. **Method for Monte Carlo Simulation of Experiments**. 21 April 2006.

[23] Schnee, Richard. **Determination of WIMP Mass (and Cross Section) with Direct Detection**. Slide presentation. *Complementarity DM Searches & Collider Expts*. June 2006.

[24] Green, Anne M. **Determining the WIMP mass using direct detection experiments**. arXiv:hep-ph/0703217v1. 20 March 2007.